JOURNAL OF THERMOPHYSICS AND HEAT TRANSFER
Vol. 19, No. 3, July–September 2005

Fluid Flow in Axial Reentrant Grooves with Application to Heat Pipes

Scott K. Thomas* and Vikrant C. Damle†
Wright State University, Dayton, Ohio 45435

The fully developed laminar flow within a reentrant groove has been analyzed using a finite element model. A parametric analysis was carried out to determine the Poiseuille number $Po = fRe$, the dimensionless mean velocity $\overline{v^*}$, and the dimensionless volumetric flow rate $\dot{V}^*$ as functions of the geometry of the reentrant groove (groove height $1.0 \le H^* \le 4.0$, slot half-width $0.05 \le W^*/2 \le 0.9$, and fillet radius $0.0 \le R_f^* \le 1.0$), and the liquid–vapor shear stress ($0.0 \le -\tau_{lv}^* \le 2.5$). The case in which the meniscus recedes into the reentrant groove was examined and could be a result of evaporator dryout or insufficient liquid fill amount. The cross-sectional area of the liquid in the groove, A_l^*, the meniscus radius R_m^*, and the aforementioned flow variables were calculated as functions of the meniscus contact angle ($0 \le \phi \le 40$ deg) and the meniscus attachment point ($0.0 \le H_l^* \le 2.75$). Finally, the results of the numerical model were used to determine the capillary limit of a low-temperature heat pipe with two different working fluids, water and ethanol, for a range of meniscus contact angles.

Nomenclature

A_g	=	total cross-sectional area of the reentrant groove, m^2
A_g^*	=	A_g/R^2
A_l	=	cross-sectional area of liquid, m^2
A_l^*	=	A_l/R^2
D_h	=	hydraulic diameter, $4A_l/P$, m
D_h^*	=	D_h/R
f	=	friction coefficient, $2\overline{\tau_w}/\rho\bar{v}^2$
H	=	distance from center of circular portion of reentrant groove to top of slot, m
H_l	=	vertical location of attachment point of meniscus to reentrant groove wall, m
$H_{l,s}$	=	vertical location of attachment point of meniscus to sinusoidal groove wall, m
H_s	=	height of sinusoidal groove, m
H_{tr}	=	height of trapezoidal groove, m
H^*	=	H/R
H_l^*	=	H_l/R
h_{fg}	=	heat of vaporization, J/kg
K	=	thermal conductivity, W/(m · K)
L_a	=	adiabatic length, m
L_c	=	condenser length, m
L_e	=	evaporator length, m
L_{eff}	=	effective heat pipe length, $L_e/2 + L_a + L_c/2$, m
N_g	=	number of grooves
n	=	coordinate normal to the liquid–vapor interface
n^*	=	n/R
P	=	wetted perimeter, m
Po	=	Poiseuille number, fRe
P^*	=	P/R
p	=	pressure, N/m^2
$\dot{Q}_{\text{cap}}$	=	capillary limit heat transport, W
$\dot{Q}_g$	=	heat transfer due to a single groove, W
$\dot{Q}_t$	=	total heat transported, $N_g\dot{Q}_g$, W
q''_{lv}	=	heat flux at the liquid–vapor interface, W/m^2
q''^*_{lv}	=	$q''_{lv}/q'''R$
q'''	=	internal volumetric heat generation, W/m^3
R	=	radius of circular portion of reentrant groove, m
Re	=	Reynolds number, $\rho\bar{v}D_h/\mu$
R_f	=	radius of fillet, m
R_m	=	radius of meniscus, m
R_v	=	radius of heat pipe vapor space, m
R_f^*	=	R_f/R
R_m^*	=	R_m/R
T	=	temperature, K
T_{sat}	=	saturation temperature, K
T^*	=	KT/R^2q'''
$\dot{V}$	=	volumetric flow rate, $\bar{v}A_l$, m^3/s
$\dot{V}^*$	=	$\mu\dot{V}/[R^4(-\mathrm{d}p/\mathrm{d}y)]$
v	=	y-direction velocity, m/s
$\bar{v}$	=	mean y-direction velocity, m/s
$\bar{v}_{l,\max}$	=	maximum mean liquid velocity, m/s
v^*	=	$\mu v/R^2(-\mathrm{d}p/\mathrm{d}y)$
$\overline{v^*}$	=	$\mu\bar{v}/R^2(-\mathrm{d}p/\mathrm{d}y)$
W	=	width of slot, m
W_l	=	width of liquid meniscus at attachment point to reentrant groove wall, m
$W_{l,s}$	=	width of liquid meniscus at attachment point to sinusoidal groove wall, m
W_s	=	width of sinusoidal groove, m
W_{tr}	=	width of trapezoidal groove, m
W^*	=	W/R
W_l^*	=	W_l/R
x, y, z	=	Cartesian coordinate directions
$x_{f,0}, z_{f,0}$	=	location of center point of circular fillet, m
x_t, z_t	=	point of tangency of fillet and circular portion of reentrant groove, m
x^*, y^*, z^*	=	$x/R, y/R, z/R$
$x_{f,0}^*$	=	$x_{f,0}/R = W^*/2 + R_f^*$
x_t^*	=	$x_t/R = x_{f,0}^*/(1 + R_f^*)$
z_0	=	location of center point of circular liquid meniscus, m
$z_{f,0}^*$	=	$z_{f,0}/R = z_t^* - (z_t^* - 1)(1 - x_{f,0}^*/x_t^*)$
z_t^*	=	$z_t/R = 1 + \sqrt{(1 - x_t^{*2})}$
z_0^*	=	z_0/R
α	=	circular segment duct half-angle, rad

Received 7 May 2004; presented as Paper 2004-2177 at the AIAA 37th Thermophysics Conference, Portland, OR, 28 June–1 July 2004; revision received 25 August 2004; accepted for publication 21 September 2004.

*Associate Professor, Department of Mechanical and Materials Engineering. Associate Fellow AIAA.

†Graduate Teaching Assistant, Department of Mechanical and Materials Engineering; currently Design Engineer, Customer Engineering Tailoring, Cummins Engine Co., Columbus, Indiana 47201.

β = aspect ratio for rectangular and trapezoidal grooves, $2H_r/W_r$ or $2H_{\rm tr}/W_{\rm tr}$
γ = triangular groove half-angle, rad
θ = trapezoidal groove half-angle, rad
μ = absolute viscosity, Pa · s
ρ = density, kg/m^3
σ = surface tension, N/m
τ_{lv} = shear stress at the liquid–vapor interface, N/m^2
τ^*_{lv} = $\tau_{lv}/R(-{\rm d}p/{\rm d}y)$
$\overline{\tau_w}$ = average shear stress at wall, N/m^2
ϕ = meniscus contact angle, rad
ϕ_0 = minimum meniscus contact angle, rad
ψ_1 = $\tan^{-1}[(W^*_l/2)/(H^*_l - 1)]$
ψ_2 = $\tan^{-1}[(W^*_l/2 - x^*_{f,0})/(H^*_l - z^*_{f,0})]$

I. Introduction

FOR years, heat pipes have been widely used for thermal control in both terrestrial and space-based applications. Heat pipes provide a high heat transfer rate with approximately isothermal behavior and self-regulating cooling characteristics. For a high heat transfer rate, the capillary structure must be designed in such a way that it combines a high capillary pumping pressure (pressure difference between the liquid and vapor sides of the meniscus) with a low axial pressure drop in the liquid. The first aim can be achieved by using small rectangular, trapezoidal, or triangular grooves. However, these structures lead to a relatively high axial pressure drop in the liquid and, therefore, the second aim cannot be fulfilled. Harwell et al.[1] described the heat transfer characteristics of an axially grooved aluminum extrusion with a reentrant groove profile. A typical cross section for this type of heat pipe is shown in Fig. 1a. This configuration combines a high capillary pumping pressure with a low axial pressure drop in the liquid.[2,3] In addition, the retardation of the liquid flow due to the countercurrent vapor flow over the liquid–vapor interface is minimized as compared to other axial groove designs. However, the radial thermal resistance to heat transfer of the reentrant groove geometry may be larger compared to rectangular, trapezoidal, or triangular groove designs due to an increase in the wall thickness of the heat pipe.

The monogroove heat pipe developed by Alario et al.[4] and Alario[5] is an aluminum extrusion with a single slot connecting the vapor channel to the liquid artery, as shown in Fig. 1b. In general, axially grooved heat pipes utilize a relatively large number of small grooves as a compromise between axial transport capacity and radial heat-transfer efficiency. In the monogroove design, the single reentrant groove is made up of the slot and the liquid artery, which returns the liquid to the evaporator section using the capillary pumping pressure generated by the meniscus residing in the slot. Circumferential grooves on the inside wall in the vapor space provide a means for liquid communication between the vapor space and the reentrant groove.[6–8] This geometry combines the advantages of a large axial artery (low-pressure drop in the liquid) with large areas for evaporation and condensation on the circumferential wall grooves. In addition, the heat input is removed as far as possible from the liquid artery, which reduces the possibility of boiling within the liquid artery, which would cause the artery to deprime. A disadvantage of the monogroove heat pipe is related to the narrow slot width, which is necessary for a high capillary pumping pressure within the slot. This causes the liquid fill amount inside the liquid channel to be so critical that a small decrease in liquid fill may result in a significant decrease in the capillary pumping pressure and, hence, a significant decrease in the maximum heat transport.

Previous researchers, for example, Harwell et al.,[1] Alario et al.,[4] Henson,[6] and Brandt et al.,[9] have modeled the flow of liquid in both reentrant groove heat pipes and in monogroove heat pipes as a one-dimensional laminar flow through a smooth-walled tube to determine the pressure drop ($Po = fRe = 16$). In addition, the effect of the shear stress at the liquid–vapor interface has not been accounted for. Whereas Brandt et al.[9] examined the effect of the liquid fill amount in the groove on the capillary pressure, only the case in which the liquid meniscus remained attached to the top of the slot

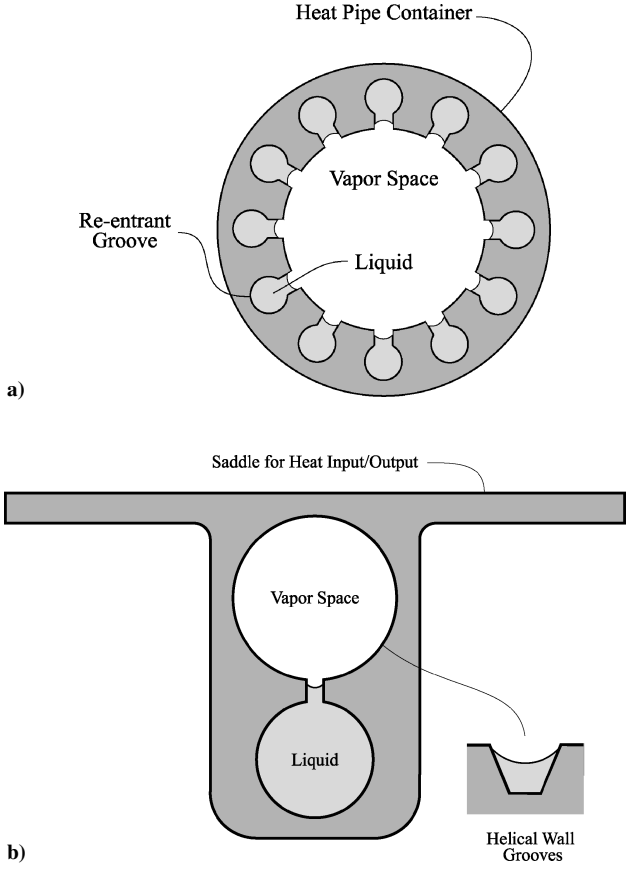

Fig. 1 Heat pipes using reentrant grooves: a) multiple reentrant grooves distributed uniformly around circumference and b) monogroove heat pipe design with single reentrant groove.

was examined. The present study has addressed these shortcomings by numerically solving the conservation of mass and momentum equations for laminar fully developed flow in reentrant grooves with an applied shear stress at the liquid–vapor interface. The meniscus contact angle, countercurrent shear stress at the liquid–vapor interface, and groove geometry were varied, and the mean velocity, Poiseuille number, and volumetric flow rate have been determined. The results of the numerical model were used in an analytical model of a heat pipe with axial reentrant grooves. The capillary limit was determined as a function of the minimum meniscus contact angle, groove fill amount, and the working fluid.

II. Mathematical Model

A constant property liquid flows steadily in a reentrant groove as shown in Fig. 2. A meniscus, which is assumed to be circular, comprises the liquid–vapor interface. The flow within the groove was modeled as being fully developed because the groove length is typically several orders of magnitude greater than the hydraulic diameter. For fully developed laminar flow with no body forces, the dimensionless conservation of mass and momentum equations reduce to[10]

$$\frac{\partial^2 v^*}{\partial x^{*2}} + \frac{\partial^2 v^*}{\partial z^{*2}} = -1 \tag{1}$$

On the groove wall, the no-slip condition is in effect:

$$v^* = 0$$

$$x^* = \begin{cases} \sqrt{z^*(2 - z^*)}, & 0 \le z^* \le z^*_t \text{ (circular region)} \\ x^*_{f,0} - \sqrt{R^{*2}_f - \left(z^* - z^*_{f,0}\right)^2}, & z^*_t \le z^* \le z^*_{f,0} \text{ (fillet region)} \\ W^*/2, & z^*_{f,0} \le z^* \le 1 + H^* \text{ (slot region)} \end{cases} \tag{2}$$

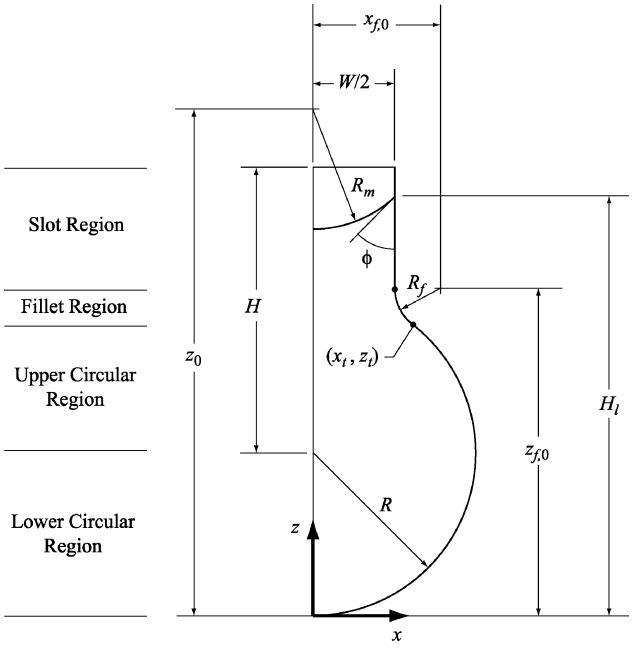

Fig. 2 Geometric parameters defining flow of liquid in reentrant groove.

At the line of symmetry, the velocity gradient is zero in the x^* direction

$$\frac{\partial v^*}{\partial x^*} = 0, \qquad x^* = 0, \qquad 0 \le z^* \le 1 + H^* \tag{3}$$

At the liquid–vapor interface, a uniform shear stress due to vapor flowing above the meniscus is imposed in the y direction,

$$\frac{\partial v^*}{\partial n^*} = \tau_{lv}^* \tag{4}$$

The dimensional liquid–vapor interfacial shear stress can be cast in terms of the friction factor of the vapor,

$$\tau_{lv} = \begin{cases} \left[\dfrac{\rho_v(\overline{v_v})^2}{2}\right] f_v, & \text{for cocurrent flow} \\ -\left[\dfrac{\rho_v(\overline{v_v})^2}{2}\right] f_v, & \text{for countercurrent flow} \end{cases} \tag{5}$$

The equation of the circular liquid meniscus is

$$x^* = \sqrt{R_m^{*2} - \left(z^* - z_0^*\right)^2} \tag{6}$$

The vertical range of this equation depends on the location of the attachment point of the meniscus to the groove wall.

For $H_l^* \le 1$ (lower circular region),

$$\begin{aligned} z_0^* - R_m^* \le z^* \le H_l^* \qquad &\text{if} \qquad \phi < -\psi_1 \\ H_l^* \le z^* \le z_0^* + R_m^* \qquad &\text{if} \qquad \phi > -\psi_1 \end{aligned} \tag{7}$$

For $H_l^* \ge 1$ (upper circular region, fillet region, and slot region),

$$z_0^* - R_m^* \le z^* \le H_l^* \tag{8}$$

The radius, half-width, and vertical location of the center point of the circular liquid meniscus are given here:

$$R_m^* = \sqrt{\left(\frac{W_l^*}{2}\right)^2 + \left(H_l^* - z_0^*\right)^2} \tag{9}$$

$$\frac{W_l^*}{2} = \begin{cases} \sqrt{H_l^*\left(2 - H_l^*\right)}, & 0 \le H_l^* \le z_t^* \text{ (circular region)} \\ x_{f,0}^* - \sqrt{R_f^{*2} - \left(H_l^* - z_{f,0}^*\right)^2}, & z_t^* \le H_l^* \le z_{f,0}^* \text{ (fillet region)} \\ \dfrac{W^*}{2}, & z_{f,0}^* \le H_l^* \le 1 + H^* \text{ (slot region)} \end{cases} \tag{10}$$

$$z_0^* = \begin{cases} H_l^* - \dfrac{\left(W_l^*/2\right)}{\tan(\phi + \psi_1)}, & 0 \le H_l^* \le z_t^* \text{ (circular region)} \\ H_l^* - \dfrac{\left(W_l^*/2\right)}{\tan(\phi + \psi_2)}, & z_t^* \le H_l^* \le z_{f,0}^* \text{ (fillet region)} \\ H_l^* + \left(\dfrac{W_l^*}{2}\right)\tan\phi, & z_{f,0}^* \le H_l^* \le 1 + H^* \text{ (slot region)} \end{cases} \tag{11}$$

The Poiseuille number of the liquid in the groove is given by

$$Po = fRe = D_h^{*2}/2v^* \tag{12}$$

The mean velocity is defined as

$$\overline{v^*} = \frac{2}{A_l^*}\int_0^{x^*}\int_0^{z^*} v^*\,\mathrm{d}z^*\,\mathrm{d}x^* \tag{13}$$

The dimensionless hydraulic diameter is

$$D_h^* = 4A_l^*/P^* \tag{14}$$

The cross-sectional area of the liquid is given in terms of the meniscus attachment point.

For $0 \le H_l^* \le 1$ (lower circular region),

$$A_l^* = \left(\frac{W_l^*}{2}\right)\left[2z_0^* - \sqrt{R_m^{*2} - \left(\frac{W_l^*}{2}\right)^2}\right] - R_m^{*2}\sin^{-1}\left(\frac{W_l^*/2}{R_m^*}\right) - \left\{\left(\frac{W_l^*}{2}\right)\left[2 - \sqrt{1 - \left(\frac{W_l^*}{2}\right)^2}\right] - \sin^{-1}\left(\frac{W_l^*}{2}\right)\right\} \qquad \text{for} \quad \phi < -\psi_1 \tag{15}$$

$$A_l^* = \left(\frac{W_l^*}{2}\right)\left[2z_0^* + \sqrt{R_m^{*2} - \left(\frac{W_l^*}{2}\right)^2}\right] + R_m^{*2}\sin^{-1}\left(\frac{W_l^*/2}{R_m^*}\right) - \left\{\left(\frac{W_l^*}{2}\right)\left[2 - \sqrt{1 - \left(\frac{W_l^*}{2}\right)^2}\right] - \sin^{-1}\left(\frac{W_l^*}{2}\right)\right\} \qquad \text{for} \quad \phi \ge -\psi_1 \tag{16}$$

For $1 \le H_l^* \le z_t^*$ (upper circular region),

$$A_l^* = \pi + \left(\frac{W_l^*}{2}\right)\left[2\left(H_l^* - 1\right) - \sqrt{1 - \left(\frac{W_l^*}{2}\right)^2}\right] - \sin^{-1}\left(\frac{W_l^*}{2}\right) + R_m^{*2}\left[\cos^{-1}\left(\frac{H_l^* - z_0^*}{R_m^*}\right) - \pi\right] - \left(H_l^* - z_0^*\right)\sqrt{R_m^{*2} - \left(H_l^* - z_0^*\right)^2} \quad \text{for} \quad \phi < \frac{\pi}{2} - \psi_1 \tag{17}$$

$$A_l^* = \pi + \left(\frac{W_l^*}{2}\right)\left[2z_0^* - \sqrt{R_m^{*2} - \left(\frac{W_l^*}{2}\right)^2}\right] - R_m^{*2}\sin^{-1}\left(\frac{W_l^*/2}{R_m^*}\right) - \left\{\left(\frac{W_l^*}{2}\right)\left[2 + \sqrt{1 - \left(\frac{W_l^*}{2}\right)^2}\right] + \sin^{-1}\left(\frac{W_l^*}{2}\right)\right\} \quad \text{for} \quad \phi \ge \frac{\pi}{2} - \psi_1 \tag{18}$$

For $z_t^* \le H_l^* \le z_{f,0}^*$ (fillet region),

$$A_l^* = \pi + W_l^* H_l^* + \left(x_t^* - x_{f,0}^*\right)\left[2z_{f,0}^* - \sqrt{R_f^{*2} - \left(x_t^* - x_{f,0}^*\right)^2}\right] - \left(\frac{W_l^*}{2} - x_{f,0}^*\right)\left[2z_{f,0}^* - \sqrt{R_f^{*2} - \left(\frac{W_l^*}{2} - x_{f,0}^*\right)^2}\right] - R_f^{*2}\left[\sin^{-1}\left(\frac{x_t^* - x_{f,0}^*}{R_f^*}\right) - \sin^{-1}\left(\frac{W_l^*/2 - x_{f,0}^*}{R_f^*}\right)\right] - x_t^*\left(2 + \sqrt{1 - x_t^{*2}}\right) - \sin^{-1}\left(x_t^*\right) + R_m^{*2} \times \left[\cos^{-1}\left(\frac{H_l^* - z_0^*}{R_m^*}\right) - \pi\right] - \left(H_l^* - z_0^*\right)\sqrt{R_m^{*2} - \left(H_l^* - z_0^*\right)^2} \quad \text{for} \quad \phi < \frac{\pi}{2} - \psi_2 \tag{19}$$

$$A_l^* = \pi + \left(\frac{W_l^*}{2}\right)\left[2z_0^* - \sqrt{R_m^{*2} - \left(\frac{W_l^*}{2}\right)^2}\right] - R_m^{*2}\sin^{-1} \times \left(\frac{W_l^*/2}{R_m^*}\right) + \left(x_t^* - x_{f,0}^*\right)\left[2z_{f,0}^* - \sqrt{R_f^{*2} - \left(x_t^* - x_{f,0}^*\right)^2}\right] - \left(\frac{W_l^*}{2} - x_{f,0}^*\right)\left[2z_{f,0}^* - \sqrt{R_f^{*2} - \left(\frac{W_l^*}{2} - x_{f,0}^*\right)^2}\right] - R_f^{*2}\left[\sin^{-1}\left(\frac{x_t^* - x_{f,0}^*}{R_f^*}\right) - \sin^{-1}\left(\frac{W_l^*/2 - x_{f,0}^*}{R_f^*}\right)\right] - x_t^*\left(2 + \sqrt{1 - x_t^{*2}}\right) - \sin^{-1}\left(x_t^*\right) \quad \text{for} \quad \phi \ge \frac{\pi}{2} - \psi_2 \tag{20}$$

For $z_{f,0}^* \le H_l^* \le 1 + H^*$ (slot region),

$$A_l^* = \pi + \left(\frac{W_l^*}{2}\right)\left[2z_0^* - \sqrt{R_m^{*2} - \left(\frac{W_l^*}{2}\right)^2}\right] - R_m^{*2}\sin^{-1}\left(\frac{W_l^*/2}{R_m^*}\right) + \left(x_t^* - x_{f,0}^*\right) \times \left[2z_{f,0}^* - \sqrt{R_f^{*2} - \left(x_t^* - x_{f,0}^*\right)^2}\right] + 2R_f^* z_{f,0}^* - R_f^{*2}\left[\sin^{-1}\left(\frac{x_t^* - x_{f,0}^*}{R_f^*}\right) + \frac{\pi}{2}\right] - x_t^*\left(2 + \sqrt{1 - x_t^{*2}}\right) - \sin^{-1}\left(x_t^*\right) \tag{21}$$

The total cross-sectional area of the reentrant groove is

$$A_g^* = \pi + W^*(1 + H^*) + \left(x_t^* - x_{f,0}^*\right) \times \left[2z_{f,0}^* - \sqrt{R_f^{*2} - \left(x_t^* - x_{f,0}^*\right)^2}\right] + 2R_f^* z_{f,0}^* - R_f^{*2}\left[\sin^{-1}\left(\frac{x_t^* - x_{f,0}^*}{R_f^*}\right) + \frac{\pi}{2}\right] - x_t^*\left(2 + \sqrt{1 - x_t^{*2}}\right) - \sin^{-1}\left(x_t^*\right) \tag{22}$$

The wetted perimeter is also given in terms of the location of the attachment point of the meniscus.

For $0 \le H_l^* \le z_t^*$ (circular region),

$$P^* = \pi + 2\tan^{-1}\left[\left(H_l^* - 1\right)/\left(W_l^*/2\right)\right] \tag{23}$$

For $z_t^* \le H_l^* \le z_{f,0}^*$ (fillet region),

$$P^* = \pi + 2\tan^{-1}\left(\frac{z_t^* - 1}{x_t^*}\right) + 2R_f^*\left[\tan^{-1}\left(\frac{W_l^*/2 - x_{f,0}^*}{H_l^* - z_{f,0}^*}\right) - \tan^{-1}\left(\frac{x_t^* - x_{f,0}^*}{z_t^* - z_{f,0}^*}\right)\right] \tag{24}$$

For $z_{f,0}^* \le H_l^* \le 1 + H^*$ (slot region),

$$P^* = \pi + 2\tan^{-1}\left(\frac{z_t^* - 1}{x_t^*}\right) + 2R_f^*\left[\frac{\pi}{2} - \tan^{-1}\left(\frac{x_t^* - x_{f,0}^*}{z_t^* - z_{f,0}^*}\right)\right] + 2\left(H_l^* - z_{f,0}^*\right) \tag{25}$$

Note that more general models of moving interfaces are available in the open literature, for example, Ref. 11.

III. Numerical Model Validation

The finite element code available to the researchers could solve the elliptic Poisson equation (1) with mixed boundary conditions (2–4) by using a simple transformation. The fluid flow problem was solved as a heat conduction problem by mapping the variables, geometry, and boundary conditions. The analogous steady-state heat conduction problem is one in which a plate of uniform thickness and constant properties has a uniform internal volumetric heat generation. The conservation of energy equation for this case is given hereafter in dimensionless form[12]:

$$\frac{\partial^2 T^*}{\partial x^{*2}} + \frac{\partial^2 T^*}{\partial z^{*2}} = -1 \tag{26}$$

The boundary conditions for the energy equation must also match those of the fluid flow problem. The temperature on the groove wall is zero,

$$T^* = 0$$

$$x^* = \begin{cases} \sqrt{z^*(2 - z^*)}, & 0 \le z^* \le z_t^* \text{ (circular region)} \\ x_{f,0}^* - \sqrt{R_f^{*2} - \left(z^* - z_{f,0}^*\right)^2}, & z_t^* \le z^* \le z_{f,0}^* \text{ (fillet region)} \\ W^*/2, & z_{f,0}^* \le z^* \le 1 + H^* \text{ (slot region)} \end{cases} \tag{27}$$

At the line of symmetry, the heat flux is zero in the x^* direction,

$$\frac{\partial T^*}{\partial x^*} = 0, \qquad x^* = 0, \qquad 0 \le z^* \le 1 + H^* \tag{28}$$

The dimensionless heat flux at the liquid–vapor interface is specified:

$$\frac{\partial T^*}{\partial n^*} = -q''^*_{lv} \tag{29}$$

The elliptic Poisson equation given by Eq. (26) with mixed boundary conditions (27–29) was solved using a finite element code. A two-dimensional planar element was used that had thermal conduction capabilities. The element had eight nodes with a single degree of freedom, temperature, at each node and was well-suited to model curved boundaries. The solution was considered to be independent of the number of elements when the Poiseuille number changed by less than 1% when the number of elements was doubled.

The numerical model was tested against existing solutions for a variety of situations to ensure the validity of the results (see Ref. 13). Shah and London[14] determined the friction factors for the laminar flow within a family of circular segment ducts using a least-squares-matching technique. A comparison of the Poiseuille number between the present solution and that given by Shah and London[14] for $8 \le 2\alpha \le 160$ deg was made, and the agreement was excellent with a maximum difference of 1.4%.

DiCola[15] solved the conservation of mass and momentum equations for the laminar flow of liquid in rectangular grooves with a uniform shear stress imposed at the liquid–vapor interface using separation of variables. The comparison of the Poiseuille number for the present solution and the solution given by DiCola[15] for $\tau^*_{lv} = -0.1$, 0, and 1.0 and $0.1 \le \beta \le 1.0$ resulted in a maximum difference of 1.2%.

Romero and Yost[16] analyzed the flow of liquid in a triangular groove with no shear stress at the liquid–vapor interface. The present solution was compared with that provided by Romero and Yost[16] for $\gamma = 5$ and 60 deg and $0.1 \le \phi \le 80$ deg, which resulted in a maximum difference of 2.6%.

Thomas et al.[17,18] solved the elliptic Poisson equation with mixed boundary conditions using Gauss–Seidel iteration with successive overrelaxation for sinusoidal and trapezoidal grooves, respectively. The results of the present solution for sinusoidal grooves are compared with those given by Thomas et al.[17] in Fig. 3 for $\phi = 0$, 25, 50, and 72.34 deg and $-0.1 \le \tau^*_{lv} \le 2.0$. The present numerical model was also compared to that given by Thomas et al.[18] for trapezoidal grooves as shown in Fig. 4 for $\phi = 0$, 20, 40, and 60 deg and $-0.375 \le \tau^*_{lv} \le 5.0$. Because of the rectangular nature of the grid used to solve the Poisson equation, the shear stress boundary condition at the liquid–vapor interface given by Eq. (4) was approximated by Thomas et al.[17,18] as follows:

$$\frac{\partial v^*}{\partial n^*} \simeq \frac{\partial v^*}{\partial z^*} = \tau^*_{lv} \tag{30}$$

In other words, the shear stress was not applied normally to the liquid–vapor interface, except when the interface was parallel to the x^* axis. In the present analysis, it was possible to apply the shear stress normally to the liquid surface using the finite element code. This caused a significant difference between the present analysis and those given by Thomas et al.[17,18] When the liquid surface was flat, that is, when the meniscus contact angle was $\phi = 72.34$ deg for the sinusoidal groove (Fig. 3b) and $\phi = 60$ deg for the trapezoidal groove (Fig. 4b), the results of the present analysis and the results obtained by Thomas et al.[17,18] were in agreement with a maximum difference of 1.4% for the sinusoidal groove and of 1.4% for the trapezoidal groove. As the meniscus contact angle decreased, the difference between the present results and those by Thomas et al.[17,18] differed by as much as 14%, as shown in Figs. 3c and 4c. This shows that the shear stress approximation considered by Thomas et al.[17,18] was the cause of the difference in the results.

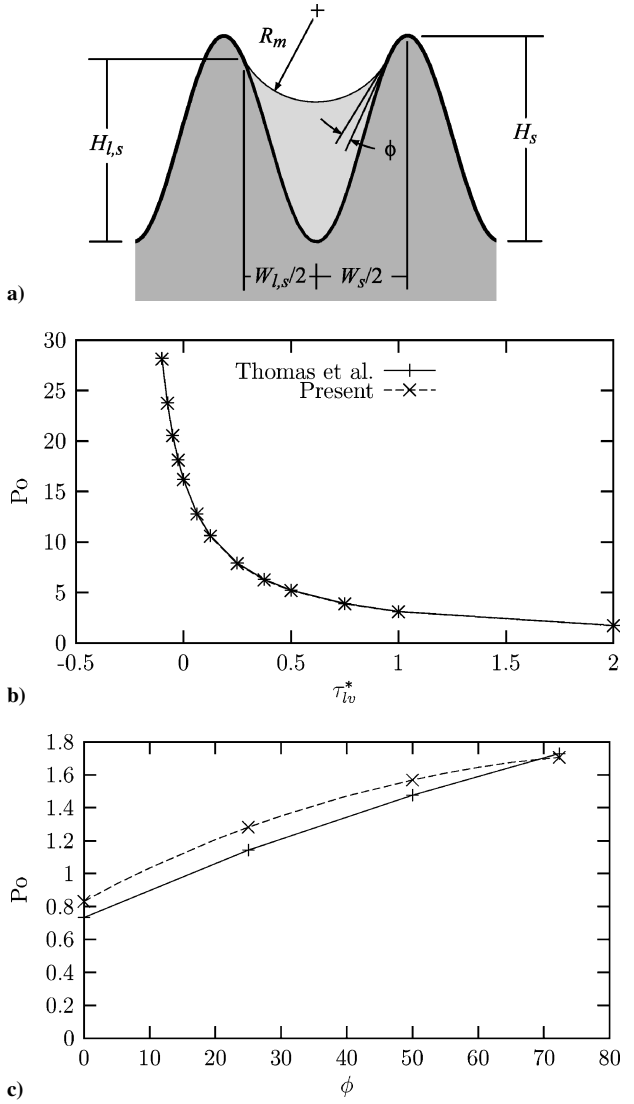

Fig. 3 Comparison of present solution with that given by Thomas et al.[17] for sinusoidal groove ($\beta = 0.5$, $W^*_{l,s}/2 = 0.25$, and $P^* = 1.15245$): a) sinusoidal groove geometry, b) Poiseuille number vs liquid–vapor shear stress ($\phi = 72.34$ deg), and c) Poiseuille number vs meniscus contact angle ($\tau^*_{lv} = 2.0$).

IV. Results and Discussion

A. Parametric Analysis

A numerical study has been completed in which the flowfield in a reentrant groove has been solved. Specifically, the mean velocity, Poiseuille number, and volumetric flow rate are reported for various values of the dimensionless shear stress at the liquid–vapor interface, groove height, slot width, and fillet radius. Figure 5 shows the dimensionless velocity in a typical reentrant groove with and without countercurrent shear stress at the free surface. For $\tau^*_{lv} = 0.0$, Fig. 5a, the maximum velocity is located slightly above the center of the circular region. In Fig. 5b, where a countercurrent shear stress ($\tau^*_{lv} = -2.5$) is imposed on the liquid–vapor interface, the velocity is at a maximum inside the circular region and is decreasing in the slot region. Because of the magnitude of the countercurrent shear at the liquid–vapor interface, the liquid near the meniscus was forced in the direction opposite to the pressure gradient.

The mean velocity, Poiseuille number, and the volumetric flow rate vs the liquid–vapor shear stress are shown in Fig. 6. The mean velocity is linear with countercurrent liquid–vapor shear stress as discussed by Thomas et al.[17] An increase in the shear stress offers more resistance to the fluid flow, which causes the mean velocity to decrease. The Poiseuille number increases monotonically with liquid–vapor shear stress as expected because the Poiseuille number

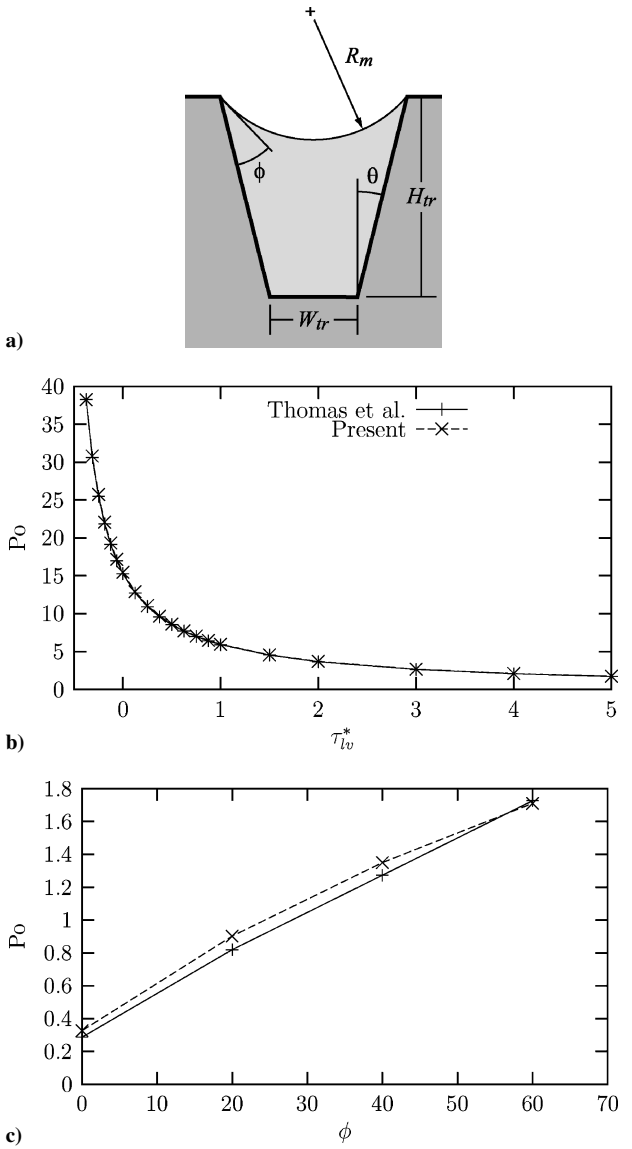

Fig. 4 Comparison of present solution with that given by Thomas et al.[18] for trapezoidal groove ($\beta = 1.0$, and $\theta = 30$ deg): a) trapezoidal groove geometry, b) Poiseuille number vs liquid–vapor shear stress ($\phi = 60$ deg), and c) Poiseuille number vs meniscus contact angle ($\tau^*_{lv} = 5.0$).

is inversely proportional to the mean velocity. The Poiseuille number increases dramatically with liquid–vapor shear stress for $H^* \leq 1.5$. This occurs because the liquid–vapor interface is much closer to the circular region, and therefore, the effect of the shear stress penetrates into the circular region more profoundly. Also, the volumetric flow rate decreases with an increase in shear stress, which is due to the decrease in mean velocity.

The variation of the three flow variables with the slot height is given in Fig. 7 for $\tau^*_{lv} = 0.0$. The mean velocity is a weak function of H^* for the range of slot half-width studied here and is nearly constant for $W^*/2 \leq 0.5$. The Poiseuille number approaches the limiting value of $Po = 16$ (circular duct) as the groove height $H^* \to 1$ and as the slot width $W^*/2 \to 0$, as expected. The mean velocity, Poiseuille number, and volumetric flow rate are affected by the slot width more significantly when the groove height is larger. For slot widths less than $W^*/2 \leq 0.3$, the volumetric flow rate does not change significantly, regardless of groove height. Because the area and mean velocity increase with both H^* and $W^*/2$, the volumetric flow rate increases in proportion.

The effect of slot width is shown in Fig. 8. The mean velocity, Poiseuille number, and volumetric flow rate are affected by

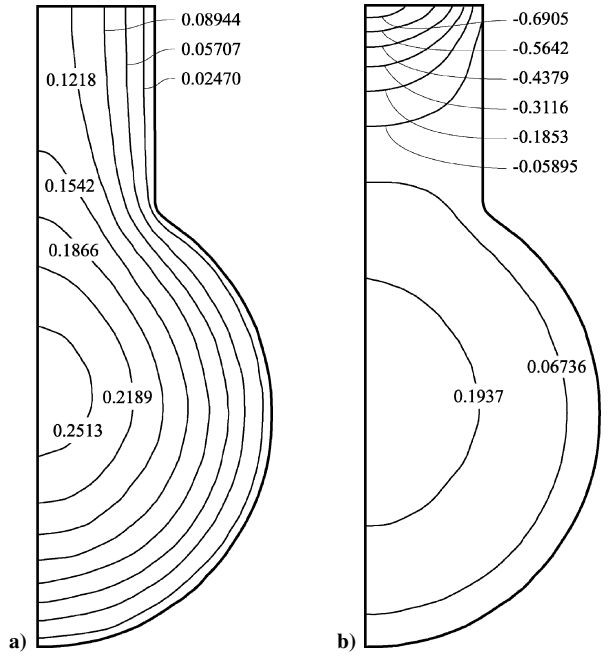

Fig. 5 Dimensionless velocity fields for laminar flow in reentrant groove ($H^* = 1.75$, $H^*_f = 2.75$, $W^*/2 = 0.5$ and $\phi = 90$ deg): a) $\tau^*_{lv} = 0.0$ and b) $\tau^*_{lv} = -2.5$.

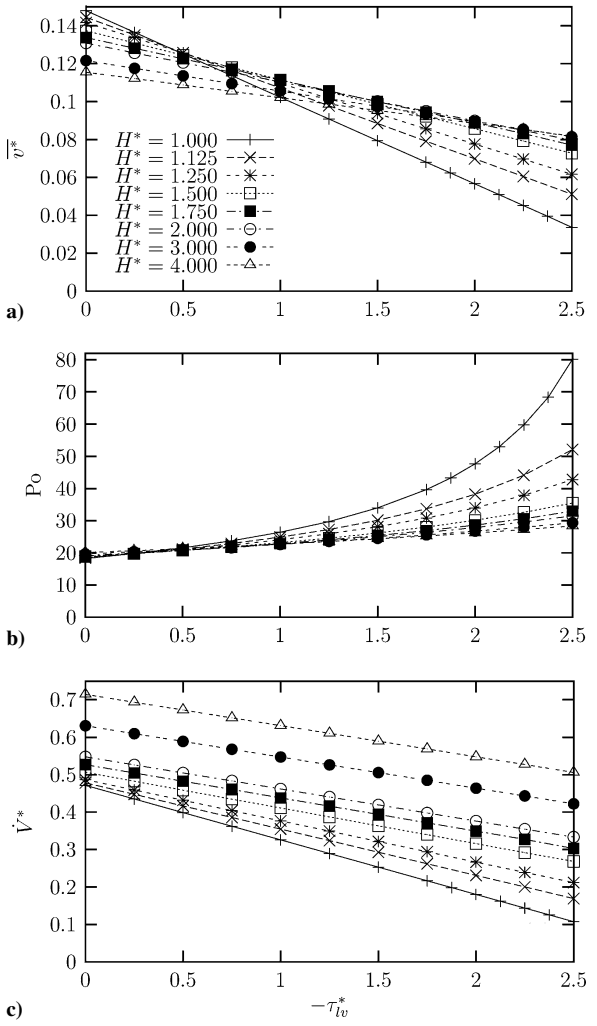

Fig. 6 Variation of flow variables with countercurrent shear stress at liquid–vapor interface ($\phi = 90$ deg, $W^*/2 = 0.5$, $R^*_f = 0.1$, and $H^*_l = H^* + 1$): a) mean velocity, b) Poiseuille number, and c) volumetric flow rate.

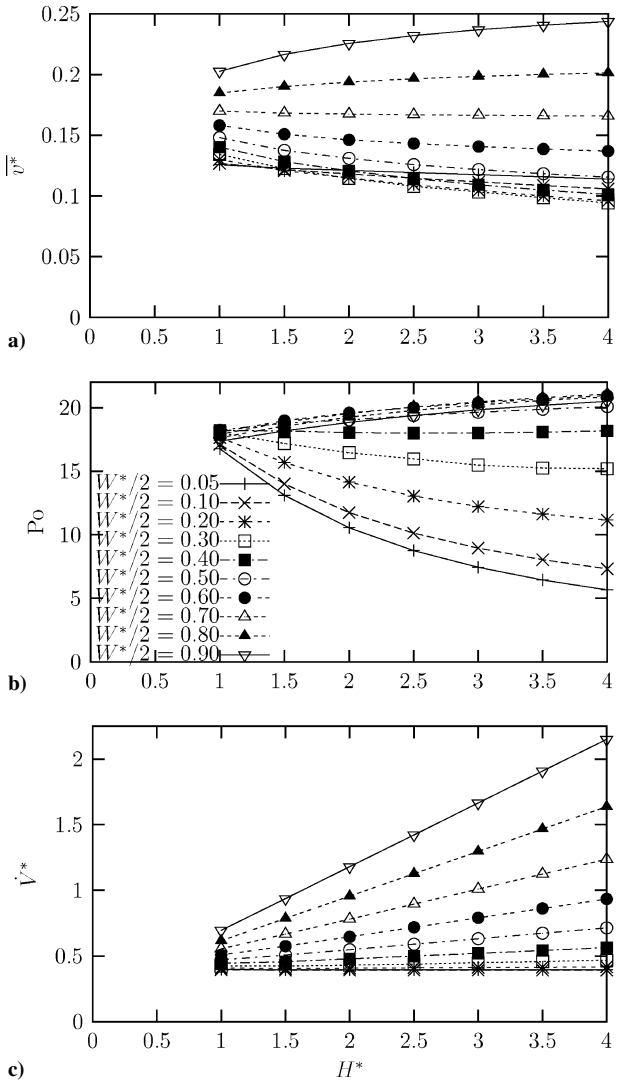

Fig. 7 Variation of flow variables with groove height ($\phi = 90$ deg, $R_f^* = 0.1$, $H_l^* = H^* + 1$, and $\tau_{lv}^* = 0.0$): a) mean velocity, b) Poiseuille number, and c) volumetric flow rate.

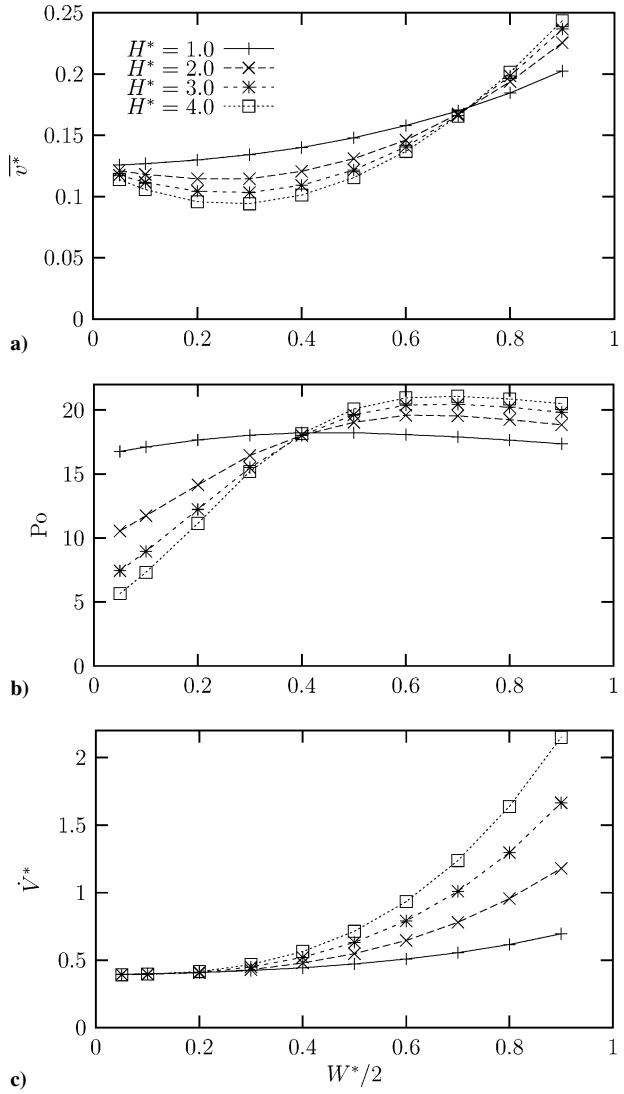

Fig. 8 Variation of flow variables with slot width ($\phi = 90$ deg, $R_f^* = 0.1$, $H_l^* = H^* + 1$, and $\tau_{lv}^* = 0.0$): a) mean velocity, b) Poiseuille number, and c) volumetric flow rate.

the slot width more significantly as the groove height increases. The Poiseuille number increases substantially with slot width for $W^*/2 \leq 0.4$ and then becomes relatively constant. The volumetric flow rate is a monotonic function of slot width, but it is nearly constant for $W^*/2 \leq 0.3$ for all values of groove height studied here. This is of interest for the monogroove-style of heat pipe, wherein the slot width is very small in comparison to the circular portion of the groove.

The effect of the fillet radius was investigated as shown to scale in Fig. 9. The variation of the flow variables with the fillet radius over a range of slot widths is shown in Fig. 10. In general, the mean velocity, Poiseuille number, and volumetric flow rate are very weak functions of the fillet radius due to the small change in liquid area with fillet radius.

B. Effect of Groove Fill Amount

The dimensions of the grooves analyzed by Brandt et al.[9] were used to determine the mean velocity, volumetric flow rate, and Poiseuille number of liquid flowing in a reentrant groove as a function of the amount of liquid in the groove. Faghri[19] gives values of the minimum meniscus contact angle for a receding meniscus for various liquids in contact with metal walls. Because the range for ϕ_0 given by Faghri is fairly large, the minimum meniscus contact angle was varied from $\phi_0 = 0$ to 40 deg.

Figure 11a shows the case when liquid evaporates from a reentrant groove with $\phi_0 = 10$ deg. Initially, the groove is full with $\phi = 90$ deg. The contact angle decreases until the minimum meniscus contact angle ϕ_0 for the particular solid–liquid combination is reached. Past this point, the meniscus detaches from the top of the groove and recedes into the groove.[20] When the meniscus reaches the fillet region of the groove, the cross-sectional area decreases dramatically for small changes in the height of the meniscus attachment point due to the requirement that the contact angle must remain constant, as shown in Fig. 12a. The decrease in liquid area is more significant in the fillet and circular regions of the groove for smaller values of ϕ_0. In fact, the liquid area $A_l^* \to 0$ when $H_l^* \to z_t^*$ for $\phi_0 = 0$ deg because the meniscus radius equals the wall radius for this case. The meniscus radius is shown as a function of the meniscus attachment point in Fig. 12b. During the meniscus recession process, after the minimum meniscus contact angle has been reached, R_m^* is constant in the slot region. In the fillet region, however, the meniscus radius may increase or decrease as the meniscus recedes further into the reentrant groove depending on ϕ_0. In all cases, as the meniscus continues to recede into the circular region, the meniscus radius increases dramatically. In the lower circular region shown in Fig. 11, the radius of curvature may approach infinity depending on the minimum meniscus contact angle and the attachment point of the meniscus to the groove wall. Past this point, the liquid in the groove can become convex instead of concave, as shown in Fig. 11b.

The flow variables vs the meniscus attachment point are presented in Fig. 13. As the liquid recedes into the groove, the mean velocity increases, attains a maximum, and then decreases to zero. The

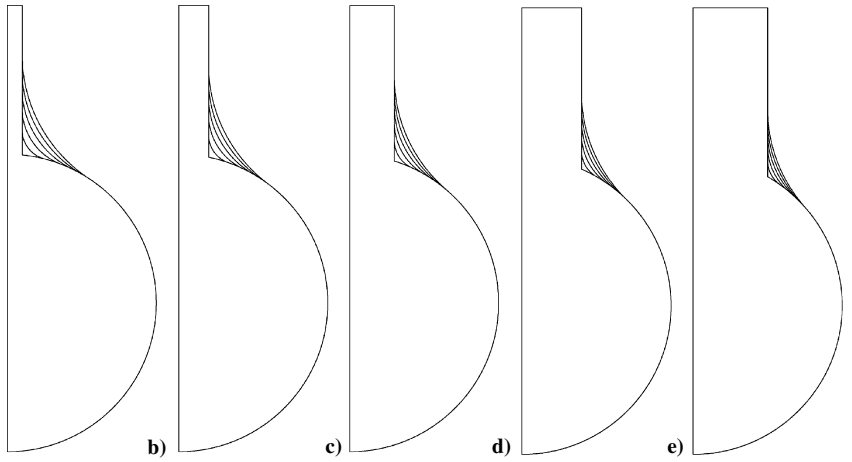

Fig. 9 Analysis of effect of fillet radius in reentrant groove (to scale) ($\phi = 90$ deg, $H^* = 2.0$, $H_l^* = 3.0$, and $\tau_{lv}^* = 0.0$): a) $W^*/2 = 0.1$, b) $W^*/2 = 0.2$, c) $W^*/2 = 0.3$, d) $W^*/2 = 0.4$, and e) $W^*/2 = 0.5$.

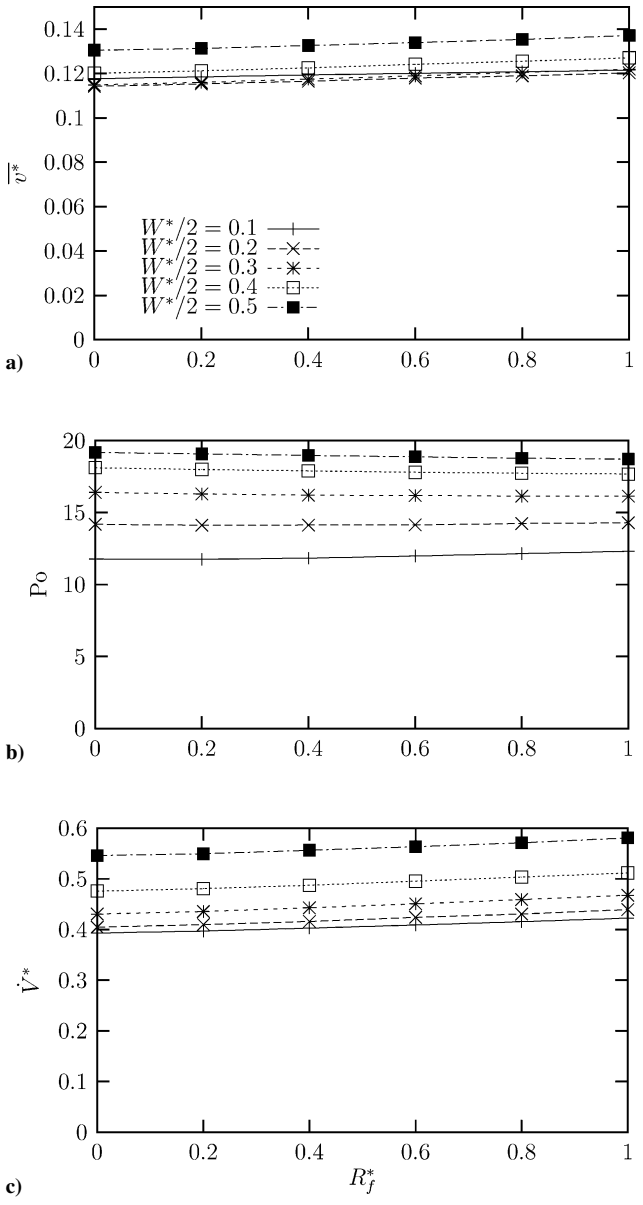

Fig. 10 Variation of flow variables with fillet radius ($\phi = 90$ deg, $H^* = 2.0$, $H_l^* = 3.0$, and $\tau_{lv}^* = 0.0$): a) mean velocity, b) Poiseuille number, and c) volumetric flow rate.

minimum meniscus contact angle does not affect the mean velocity significantly until the meniscus reaches the upper circular region, as shown in Fig. 13a. In Fig. 13b, the Poiseuille number is relatively constant in the slot region for a given meniscus contact angle and then decreases in the fillet region due to the sharp decrease in the liquid cross-sectional area. This point can be seen by recasting the Poiseuille number in terms of the liquid area by combining Eqs. (12) and (14):

$$Po = 8A_l^{*2} \Big/ P^* \overline{v^*} \tag{31}$$

The volumetric flow rate is shown in Fig. 13c, where the flow rate decreases steadily in the slot region and then decreases very quickly in the fillet region, which follows the trend in the mean velocity. The flow variables are also presented in Fig. 14 vs the groove fill amount. Note that the dimensionless volumetric flow rate for all of the meniscus contact angles studied here nearly collapse to a single curve.

C. Capillary Limit Analysis for a Heat Pipe Using Axial Reentrant Grooves

By the use of the results of the numerical analysis, the capillary limit prediction for a heat pipe with reentrant grooves is proposed. The objective is to use the results of the analysis on the effect of groove fill amount to determine the sensitivity of the performance of the heat pipe with groove fill and minimum meniscus contact angle. It is assumed that no body forces act on the liquid in the grooves, that the radius of the liquid meniscus is constant along the length of the groove, and that the liquid–vapor shear stress is negligible.

A pressure balance within the heat pipe results in the following expression for the capillary limit[19,21]

$$\Delta p_{\text{cap,max}} \geq \Delta p_v + \Delta p_l \tag{32}$$

The capillary pressure for an axial groove is

$$\Delta p_{\text{cap,max}} = 2\sigma / R_m \tag{33}$$

For a circular cross section heat pipe with uniform heat input and output along the lengths of the evaporator and condenser, respectively, the pressure drop in the vapor is

$$\Delta p_v = \frac{8\mu_v L_{\text{eff}} \dot{Q}_t}{\pi \rho_v h_{fg} R_v^4} \tag{34}$$

The Poiseuille number of the vapor flow was modeled as a laminar flow within a smooth tube with a circular cross section ($Po_v = 16$).

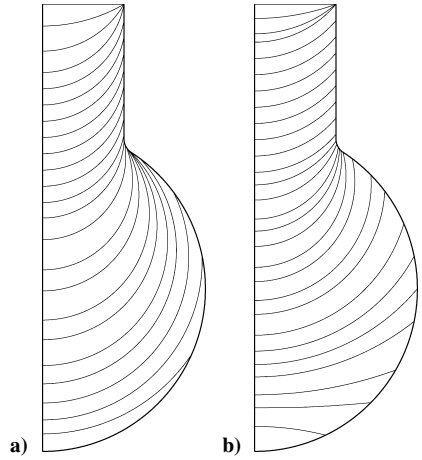

Fig. 11 Analysis of liquid fill amount in reentrant groove (to scale) ($H^* = 1.75$, $W^*/2 = 0.5$, and $R_f^* = 0.1$: a) $\phi_0 = 10$ deg and b) $\phi_0 = 40$ deg.

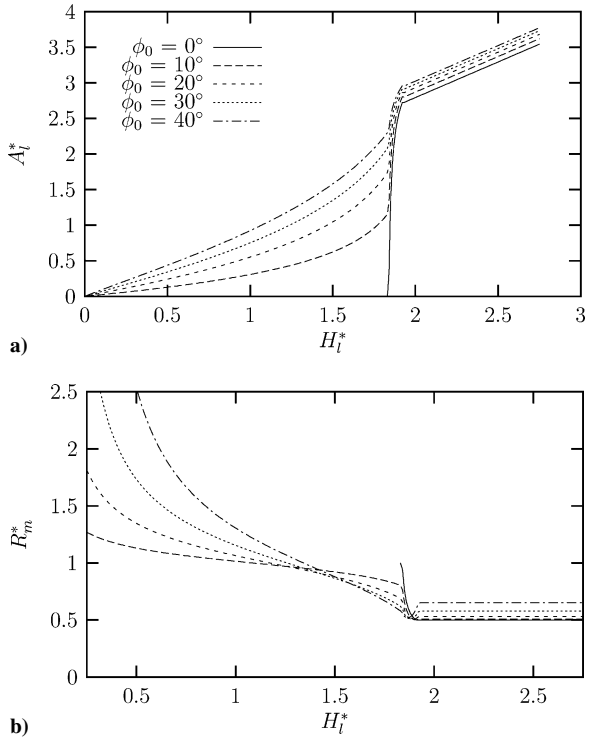

Fig. 12 Variation of geometric properties with meniscus attachment point ($H^* = 1.75$, $W^*/2 = 0.5$, and $R_f^* = 0.1$): a) liquid cross-sectional area and b) meniscus radius.

The pressure drop in the liquid was found using the dimensionless mean velocity determined by the numerical model:

$$\mathrm{d}p_l = -\left(\mu_l \overline{v_l} \Big/ R^2 \overline{v^*}\right) \mathrm{d}y \tag{35}$$

For a constant heat flux in both the evaporator and condenser sections, Eq. (35) can be integrated to determine the total pressure drop in the reentrant groove:

$$\Delta p_l = L_{\text{eff}} \left(\mu_l \bar{v}_{l,\max} \Big/ R^2 \overline{v^*}\right) \tag{36}$$

The maximum liquid velocity in a groove is in the adiabatic section:

$$\bar{v}_{l,\max} = \dot{Q}_g / \rho_l A_l h_{fg} \tag{37}$$

A closed-form solution for the capillary limit of a heat pipe with reentrant axial grooves and no body forces is

$$\dot{Q}_{\text{cap}} = \frac{2\sigma h_{fg}}{R_m L_{\text{eff}}} \left(\frac{\mu_l}{N_g R^4 \rho_l \dot{V}^*} + \frac{8\mu_v}{\pi \rho_v R_v^4} \right)^{-1} \tag{38}$$

Table 1 Specifications of reentrant groove heat pipe

Parameter	Value
Evaporator length	$L_e = 15.2 \times 10^{-2}$ m
Adiabatic length	$L_a = 8.2 \times 10^{-2}$ m
Condenser length	$L_c = 15.2 \times 10^{-2}$ m
Radius of heat pipe vapor space	$R_v = 8.59 \times 10^{-3}$ m
Radius of circular portion of groove	$R = 0.8 \times 10^{-3}$ m
Groove height	$H = 1.4 \times 10^{-3}$ m
Slot half-width	$W/2 = 0.4 \times 10^{-3}$ m
Number of grooves	$N_g = 15$
Operating temperature	$T_{\text{sat}} = 60°\text{C}$

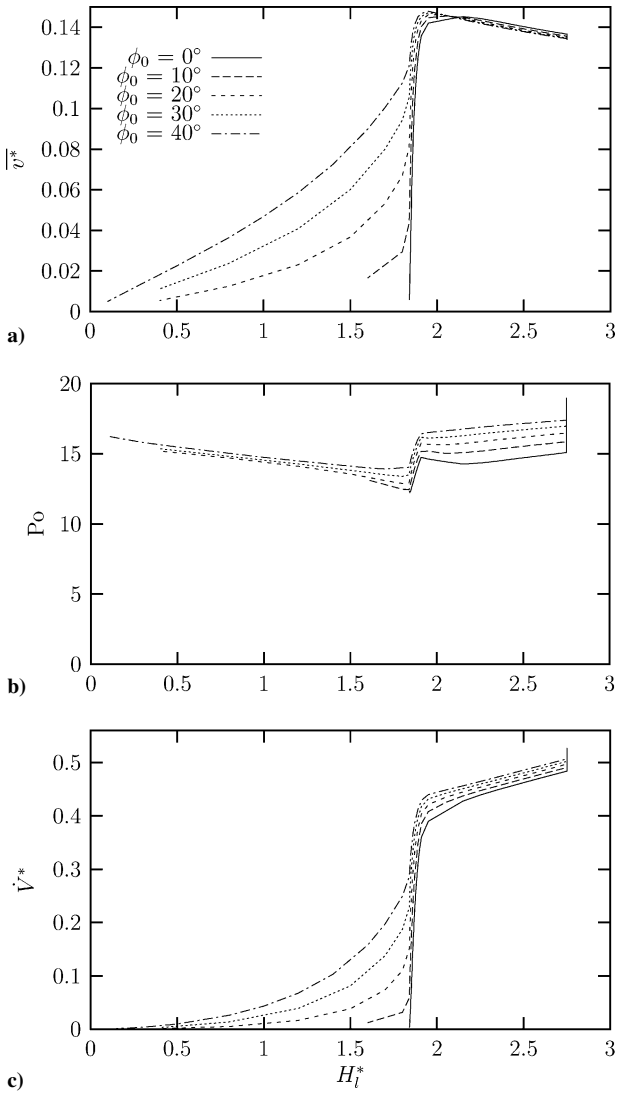

Fig. 13 Effect of meniscus attachment point on flow variables for reentrant groove ($H^* = 1.75$, $W^*/2 = 0.5$, $R_f^* = 0.1$, and $\tau_{lv}^* = 0.0$): a) mean velocity, b) Poiseuille number, and c) volumetric flow rate.

Equation (38) was evaluated using the results of the analysis for the effect of groove fill amount for the heat pipe presented in Table 1. The properties of water and ethanol were found by evaluating the temperature-dependent equations provided by Faghri.[19] The capillary limit heat transport is shown vs the meniscus attachment point in Fig. 15 and vs the groove fill amount in Fig. 16. When the groove is completely full, with $\phi = 90$ deg, the capillary limit is zero due to the infinite meniscus radius. The capillary limit quickly increases as the contact angle decreases to the minimum meniscus contact angle, at which point $\dot{Q}_{\text{cap}}$ begins to fall off due to the decrease in volumetric flow rate. The maximum value of the capillary limit is greater for smaller values of meniscus contact angle, as expected.

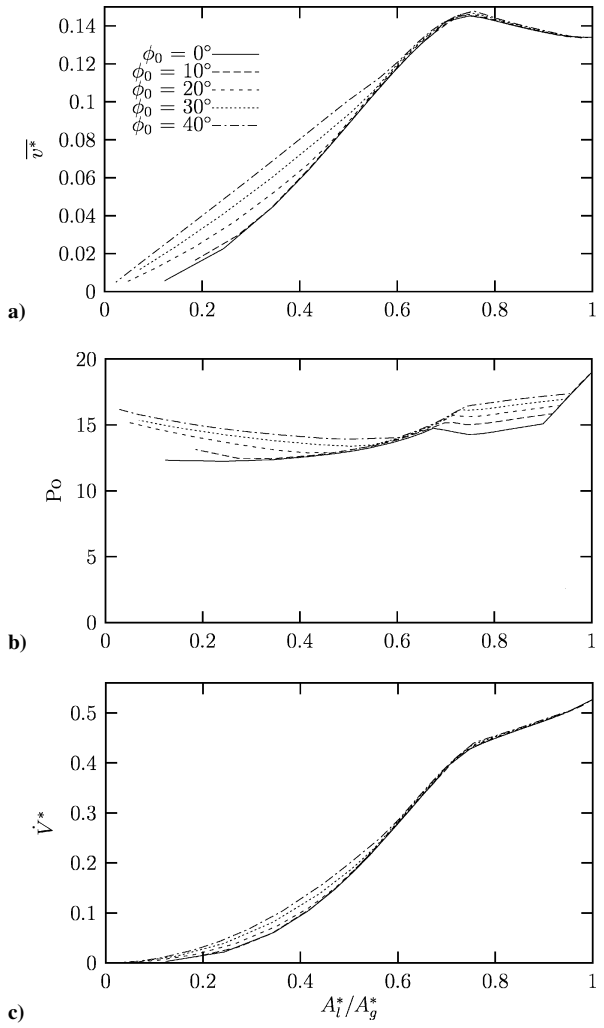

Fig. 14 Effect of liquid fill amount on flow variables for reentrant groove ($H^* = 1.75$, $W^*/2 = 0.5$, $R_f^* = 0.1$, and $\tau_{lv}^* = 0.0$): a) mean velocity, b) Poiseuille number, and c) volumetric flow rate.

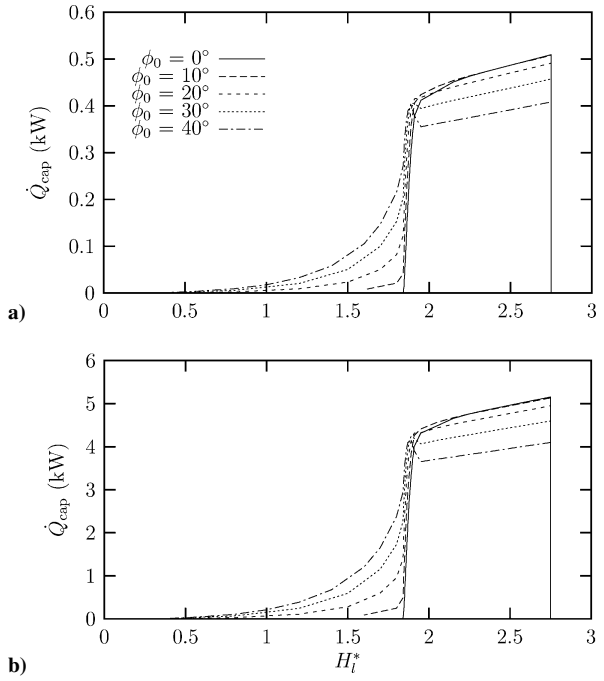

Fig. 15 Heat transport vs meniscus attachment point for different values of minimum meniscus contact angle ($H^* = 1.75$, $W^*/2 = 0.5$, $R_f^* = 0.1$, and $\tau_{lv}^* = 0.0$): a) ethanol and b) water.

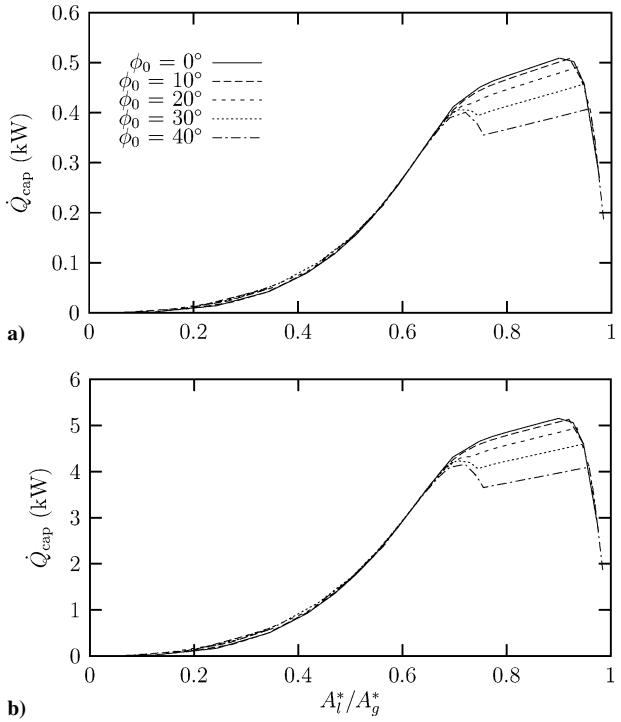

Fig. 16 Heat transport vs liquid fill amount for different values of minimum meniscus contact angle ($H^* = 1.75$, $W^*/2 = 0.5$, $R_f^* = 0.1$, and $\tau_{lv}^* = 0.0$): a) ethanol and b) water.

Figure 15 clearly shows that when the liquid recedes into the fillet region, the heat transport decreases rapidly, which demonstrates the importance of proper fluid fill amount in this type of heat pipe.

V. Conclusions

A study has been completed wherein the Poiseuille number, mean velocity, and volumetric flow rate of a liquid in a reentrant groove have been determined as functions of groove geometry, meniscus contact angle, and liquid–vapor shear stress. In addition, the effects of meniscus recession were discussed and related to the performance of a heat pipe with axial reentrant grooves. The main conclusions from this study are as follows:

1) By the use of the finite element model, it was possible to apply the countercurrent shear stress boundary condition normally to the liquid meniscus, which gave more accurate results than those obtained by a finite difference model used by some of the previous researchers.[17,18] The error in the Poiseuille number was found to be up to 14% for trapezoidal grooves and sinusoidal grooves. Also, the computer resources required by the finite element model were much less compared to those required by the finite difference model.

2) The results of the parametric analysis of the reentrant groove showed that the Poiseuille number was greatly affected by the liquid–vapor shear stress, groove height, and slot half-width, but was relatively insensitive to the fillet radius. Significant errors in the prediction of the liquid pressure drop in an axial reentrant groove would be induced by assuming that the Poiseuille number was the same as that for a smooth tube ($Po = 16$). Therefore, it is recommended that the Poiseuille number be evaluated using the methodology outlined in this paper, particularly if countercurrent vapor flowing above the meniscus imparts a significant shear stress on the liquid meniscus.

3) The volumetric flow rate for slot half-widths of $W^*/2 \leq 0.3$ approached a fairly constant value of $\dot{V}^* = 0.41$ for the groove height ranging from $1.0 \leq H^* \leq 4.0$ for a full groove with no shear stress at the meniscus. This could be important to heat pipe designers for use with the analytical prediction of the capillary limit provided in Eq. (38).

4) The capillary limit heat transfer attained a maximum value in the slot region and decreased dramatically as the meniscus receded into the circular region of the reentrant groove. This shows

the critical nature of the fluid fill amount in heat pipes with axial reentrant grooves.

References

[1]Harwell, W., Kaufman, W., and Tower, L., "Reentrant Groove Heat Pipe," *Proceedings of the 12th AIAA Thermophysics Conference*, AIAA, New York, 1977, pp. 131–147.

[2]Dubois, M., van Oost, S., Bekaert, G., and Supper, W., "High Capacity Grooved Heat Pipes," *Proceedings of the 4th European Symposium on Space Environmental Control Systems*, 1991, pp. 575–581.

[3]Dubois, M., Mullender, B., and Supper, W., "Space Qualification of High Capacity Grooved Heat Pipes," Society of Automotive Engineers, SAE Paper 972453, Warrendale, PA, July 1997.

[4]Alario, J., Haslett, R., and Kosson, R., "Monogroove High-Performance Heat Pipe," AIAA Paper 81-1156, June 1984.

[5]Alario, J., "Monogroove Heat Pipe Radiator Shuttle Flight Experiment: Design, Analysis and Testing," Society of Automotive Engineers, SAE Paper 840950, Warrendale, PA, July 1984.

[6]Henson, R., "Thermohydraulic Modelling of a Monogroove Heat Pipe Condensor," M.S. Thesis, Dept. of Mechanical and Aerospace Engineering, North Carolina State Univ., Raleigh, NC, 1998.

[7]Brown, R., Kosson, R., and Ungar, E., "Design of the SHARE II Monogroove Heat Pipe," AIAA Paper 91-1359, June 1991.

[8]Schlitt, R., "Performance Characteristics of Recently Developed High-Performance Heat Pipes," *Heat Transfer Engineering*, Vol. 16, No. 1, 1995, pp. 44–52.

[9]Brandt, C., Stephan, P., Dubois, M., and Mullender, B., "Theoretical Investigation of Advanced Capillary Structures in Grooved Heat Pipe Evaporators for Space Applications," Society of Automotive Engineers, SAE Paper 2000-01-2319, Warrendale, PA, July 2000.

[10]White, F., *Viscous Fluid Flow*, 2nd ed., McGraw–Hill, New York, 1991, pp. 115, 116.

[11]Wang, L., "Thermodynamics of Moving Gibbs Dividing Surfaces," *Physical Review E*, Vol. 55, No. 2, 1997, pp. 1732–1738.

[12]Incropera, F., and DeWitt, D., *Fundamentals of Heat and Mass Transfer*, 4th ed., Wiley, New York, 1996, Chap. 4.

[13]Damle, V., "Analysis of Fluid Flow in Axial Re-Entrant Grooves with Application to Heat Pipes," M.S. Thesis, Dept. of Mechanical and Materials Engineering, Wright State Univ., Dayton, OH, March 2004.

[14]Shah, R., and London, A., *Laminar Flow Forced Convection in Ducts*, Academic, New York, 1978, pp. 264, 265.

[15]DiCola, G., "Soluzionne Analitica, Amezzo Della Transformata di Fourier, di un Problema di Fusso in un Canale Rettangolare," *Euratom C.C.R.*, Ispra, Italy, C.E.T.I.S., 1968.

[16]Romero, L., and Yost, F., "Flow in an Open Channel," *Journal of Fluid Mechanics*, Vol. 322, 1996, pp. 109–129.

[17]Thomas, S., Lykins, R., and Yerkes, K., "Fully-Developed Laminar Flow in Sinusoidal Grooves," *Journal of Fluids Engineering*, Vol. 123, Sept. 2001, pp. 656–661.

[18]Thomas, S., Lykins, R., and Yerkes, K., "Fully Developed Laminar Flow in Trapezoidal Grooves with Shear Stress at the Liquid–Vapor Interface," *International Journal of Heat and Mass Transfer*, Vol. 44, 2001, pp. 3397–3412.

[19]Faghri, A., *Heat Pipe Science and Technology*, Taylor and Francis, Washington, DC, 1995, pp. 226, 227.

[20]Hopkins, R., Faghri, A., and Khrustalev, D., "Flat Miniature Heat Pipes with Micro Capillary Grooves," *Journal of Heat Transfer*, Vol. 121, No. 1, 1999, pp. 102–109.

[21]Chi, S., *Heat Pipe Theory and Practice: A Sourcebook*, Hemisphere, New York, 1976.